Colorimetric detection of chromium (VI) ion using poly(N-phenylglycine) nanoparticles acting as a peroxidase mimetic catalyst

Sena Ghayyem, Abir Swaidan, Alexandre Barras, Mathias Dolci, Farnoush Faridbod, Sabine Szunerits, Rabah Boukherroub

Version of Record: https://www.sciencedirect.com/science/article/pii/S0039914021000035
Manuscript_5d87e5d55f421673f89bb97f017025ba

Colorimetric detection of chromium (VI) ion using poly(N-phenylglycine) nanoparticles acting as a peroxidase mimetic catalyst

Sena Ghayyem,[1,2] Abir Swaidan,[1] Alexandre Barras,[1] Mathias Dolci,[1] Farnoush Faridbod,[2] Sabine Szunerits[1] and Rabah Boukherroub[1*]

[1]*Univ. Lille, CNRS, Centrale Lille, Univ. Polytechnique Hauts-de-France, UMR 8520 - IEMN, F-59000 Lille, France*

[2]*Analytical Chemistry Department, School of Chemistry, College of Science, University of Tehran, Tehran, Iran*

*To whom correspondence should be addressed: Rabah Boukherroub, e-mail: rabah.boukherroub@univ-lille.fr; Tel: +333 62 53 17 24

Abstract

This paper reports on enzyme-like catalytic properties of polyethylene glycol-functionalized poly(N-phenylglycine) (PNPG-PEG) nanoparticles, which has not been explored to date. The developed nanoparticles have the ability to display great inherent peroxidase-like activity at very low concentrations, and are able to catalyze the oxidation of 3,3',5,5'-tetramethylbenzidine (TMB) substrate in presence of hydrogen peroxide (H_2O_2). The oxidized product of TMB has a deep blue color with a maximum absorbance at ~655 nm. The PNPG-PEG nanoparticles exhibit K_m values of 0.2828 for TMB and 0.0799 for H_2O_2, indicating that TMB oxidation takes place at lower concentration of H_2O_2 in comparison to other nanozymes. Based on the known mechanism of H_2O_2 oxidation by hexavalent chromium [Cr(VI)] ions to generate hydroxyl radicals ($^{\bullet}OH$), these nanoparticles were successfully applied for the colorimetric sensing of Cr(VI) ions. The sensor achieved good performance for Cr(VI) sensing with detection limits of 0.012 µM (0.01-0.1 µM linear range) and 0.52 µM (0.05-12.5 µM linear range). The detection scheme was highly selective, and successfully applied for the detection of Cr(VI) in real water samples.

Keywords: Poly(N-phenylglycine) nanoparticles; peroxidase-like activity; heavy metals ion; chromium(VI) ion; colorimetric detection.

1. Introduction

Heavy metals are naturally occurring elements, capable to induce toxicity even at low doses and thus represent a serious threat for public health [1]. Therefore, detection of heavy metal ions attracted attention worldwide. Among the heavy metals, hexavalent chromium (Cr(VI)) is known as one of the most common and harmful water pollutant [2]. Cr(VI) has been widely used for various industrial applications such as wood preservation, chrome-plating, printing, stainless steel manufacture, electroplating, pigment production, leather tanning, metal-ceramic and metallurgy [3-5]. According to the U.S. Environmental Protection Agency (EPA), the acceptable chromium concentration in drinking water is ~100 μg/L, while the World Health Organization (WHO) suggests a permitted concentration of chromium in drinking water of ~50 μg/L [6, 7]. Therefore, much attention has been devoted to the development of selective and sensitive detection techniques, which are necessary for the accurate monitoring of Cr(VI) content in water.

Cr(VI) ions determination and quantification can be achieved using various analytical techniques including electrochemistry [8-10], chemiluminescence [11, 12], fluorescence [13, 14] atomic absorption spectrometry (AAS) [15, 16], gas chromatography-chromium-based high-temperature conversion (Cr/HTC)-isotope ratio mass spectrometry [17], and liquid chromatography-inductively coupled plasma-mass spectrometry (ICP-MS) [18, 19]. Even though some of these techniques allow Cr(VI) detection with high sensitivity and accuracy, their practical applications are hampered by some of their intrinsic disadvantages, such as requiring specific expertise, large equipment and long sample pretreatment processes.

In this context, colorimetric detection of Cr(VI) represents a viable and rapid analytical method [20, 21], owing to its simplicity, sensitivity, and low detection limit. In recent years, nanoparticles are used as enzyme mimics for sensing various analytes of interest. These sensors explore the enzyme-like activity of various nanomaterials that can catalyze the

oxidation of a chromogenic substrate, 3,3',5,5'-tetramethylbenzidine (TMB), into a blue colored ox-TMB molecule in the presence of H_2O_2 [22-24]. Thereby, the development of nanotechnology permitted the application of nanomaterials as enzyme mimics, commonly named nanozymes, and offers great advantages over natural enzymes.

It has been acknowledged that, during the catalytic oxidation of the enzyme substrate (TMB) in presence of H_2O_2, hydroxyl radicals ($HO^{\bullet}$) intermediates are involved in the peroxidase-like oxidation process [23, 24]. It is also well known that Cr(VI) promotes H_2O_2 decomposition into molecular O_2 and H_2O in acidic media. Electron transfer from the nanozyme into the reaction medium will promote hydroxyl radicals' generation. Thus, it is expected that Cr(VI) ions will enhance H_2O_2 decomposition to hydroxyl radicals and therefore promote the enzyme-like oxidation of TMB. Indeed, this mechanism has been recently exploited for the colorimetric detection of Cr(VI) ions by exploiting the enzyme-like properties of Cu(0) nanoparticles [23], and CuS-BSA nanostructures [25]. Similarly, the enhanced fluorescence emission intensity of hydroxyl-terephthalic acid, generated by the reaction of hydroxyl radicals with terephthalic acid (TA) in presence of TMB, H_2O_2, CuS and Cr(VI) ions, was investigated for fluorescence sensing of Cr(VI) ions with a good performance [26].

While the burgeoning field of nanozymes using inorganic nanomaterials has experienced a huge development for colorimetric detection of various species, the utilization of organic nanoparticles as enzyme mimics is relatively scarce. The first application of conducting organic polymers as a peroxidase mimics is the one reported by Liu et al. using poly[2-(3-thienyl)ethyloxy-4-butylsulfonate] (PTEBS), an anionic polythiophene derivative [27]. The peroxidase-like activity of PTEBS was applied for glucose detection with good sensitivity (4 μM) and selectivity. Following this report, Tao et al. demonstrated the enzyme-like activity of polypyrrole (PPy) nanoparticles even though the catalytic activity was assigned to the

presence of trace Fe in the nanoparticles [28]. Apart from these studies, conducting polymers were mostly investigated in their hybridized forms with metal or metal oxide nanoparticles to improve their peroxidase-like activity [29].

Poly(N-phenylglycine) (PNPG) is an analogue of polyaniline (PANI), obtained by N-phenylglycine (NPG) polymerization. While PNPG is not water dispersible, its dispersion in aqueous media can be improved through chemical functionalization with polyethylene glycol amine (PEG) [30]. In this work, we synthesized water dispersible PNPG-PEG nanoparticles and studied, for the first time, their enzyme-like activity for TMB oxidation. We demonstrated that these nanoparticles have good affinity for TMB and H_2O_2 in comparison to other nanocomposites and nanoparticles reported so far. The excellent enzyme-like activity of these nanoparticles was further exploited for the design of a low cost and sensitive method for Cr(VI) ions sensing through mixing PNPG-PEG nanoparticles, H_2O_2 and TMB to generate a blue colored 3,3',5,5'-tetramethylbenzidine diimine (TMBDI) cations. A low detection limit of 12 nM over a linear range from 0.01 to 0.1 µM was achieved under optimal experimental conditions. The technique was highly selective and successfully applied for sensing toxic Cr(VI) ion in environmental water samples.

2. Materials and Methods

2.1. Materials

Methoxypolyethylene glycol amine (PEG 750), N-phenylglycine (NPG, 97%), 1-ethyl-3-(3-dimethylaminopropyl) carbodiimide hydrochloride (EDC.HCl, ≥99.0%), 1-hydroxy-2,5-pyrrolidinedione (NHS, 98%), ammonium peroxydisulfate (APS, ≥98.0%), 3,3',5,5'-tetramethylbenzidine (TMB, ≥95.0%), terephthalic acid (TA, 98.0%), sodium acetate anhydrous (CH_3COONa, >99%), sodium hydroxide (NaOH, ≥97.0%), isopropanol ($(CH_3)_2CHOH$, ≥99.5%), potassium dichromate ($K_2Cr_2O_7$, 99.98%), cobalt (II) chloride hexahydrate ($CoCl_2 \cdot 6H_2O$, ≥99.9%), copper (II) chloride ($CuCl_2$, ≥99.995%), zinc chloride

($ZnCl_2$, ≥99.995%), calcium chloride ($CaCl_2$, ≥99.9%), sodium chloride (NaCl, ≥99.9%), palladium (II) chloride ($PdCl_2$, ≥99%), nickel (II) chloride hexahydrate ($NiCl_2 \cdot 6H_2O$, ≥99.9%), manganese (II) chloride tetrahydrate ($MnCl_2 \cdot 4H_2O$, ≥99%), magnesium chloride hexahydrate ($MgCl_2 \cdot 6H_2O$, ≥99%), chromium (III) chloride hexahydrate ($CrCl_3 \cdot 6H_2O$, ≥96%) and iron (III) chloride hexahydrate ($FeCl_3 \cdot 6H_2O$, ≥99%) were obtained from Sigma-Aldrich. Hydrogen peroxide (H_2O_2, 30 wt%,), sulfuric acid (H_2SO_4, 95%), glacial acetic acid (CH_3COOH, ≥99.85%), hydrochloric acid (HCl, 37%), and dimethylsulfoxide (DMSO) were purchased from Fisher Scientific.

2.2. Synthesis of poly(N-phenylglycine) (PNPG) nanoparticles

PNPG nanoparticles (NPs) synthesis was carried out as follows. First, N-phenylglycine (NPG, 1.06 g) and ammonium peroxydisulfate (APS, 1.6 g) were dissolved separately in 0.1 M H_2SO_4 aqueous solution (50 mL). Then, the APS solution was added slowly to the NPG solution at 0 °C (ice-water bath) over 1 h under stirring. The reaction was continued in ice-water bath for 24 h to yield a dark-green precipitate, which was filtered and washed copiously with water. Finally, the PNPG NPs were dried in an oven at 60°C overnight.

2.3. Synthesis of PNPG-PEG nanoparticles

First, 25.5 mg of PNPG were dispersed in 8.5 mL of DMSO. Then, 1-ethyl-3-(3-dimethylaminopropyl) carbodiimide hydrochloride (EDC.HCl, 161.5 mg) and 1-hydroxy-2,5-pyrrolidinedione (NHS, 97.75 mg) were added under stirring and the reaction was continued for 4 h. To this mixture, 1.2 mL of PEG 750 (22 mg/mL in water) were added dropwise and held under stirring for another 24 h. The particles were separated by centrifugation (14,600 rpm, 20 min) and rinsed sequentially with ethanol and water. Finally, the precipitate was freeze-dried to produce PNPG-PEG nanoparticles.

2.4. Determination of peroxidase-like activity of PNPG-PEG nanoparticles

The enzyme-mimetic action of PNPG-PEG NPs towards 3,3',5,5'-tetramethylbenzidine (TMB) oxidation was assessed by mixing 25 µg/mL of PNPG-PEG as a catalyst, 7.5 mM of H_2O_2 and 2 mM TMB. The reaction mixture was kept at 35°C for 30 min in acetate buffer (0.1 M, pH 4) at a final volume of 1.5 mL. Acetate buffer was prepared by mixing sodium acetate (0.93 g) and acetic acid (2.321 g) in 500 mL deionized water, and the solution pH was adjusted by using HCl or NaOH. The absorbance of TMBDI at 655 nm was monitored using UV-vis spectrophotometry in the 500-750 nm range.

The influence of catalyst concentration (10-200 µg/mL), H_2O_2 (0.1-15 mM), TMB (0.2-3 mM), reaction time (5-30 min), temperature (25-55 °C), and pH (2-10) on the enzyme-like catalytic reaction was assessed to set the optimal conditions.

To study the influence of PNPG-PEG nanoparticles concentration on the catalytic reaction, 150 µL of TMB (10 mM) and 300 µL of H_2O_2 (100 mM) were added to different concentrations (10-200 µg/mL) of PNPG-PEG and the reaction mixture was kept at 25°C for 30 min in acetate buffer (0.1 M, pH 4) at a final volume of 1.5 mL.

To optimize the concentration of TMB, 37.5 µL of PNPG-PEG (1 mg/mL) and 300 µL of H_2O_2 (100 mM) were added to different concentrations (0.2-3 mM) of TMB in acetate buffer (pH 4) at a final volume of 1.5 mL, and the reaction mixture was kept at 25 °C for 30 min.

To determine the optimum concentration of H_2O_2, 37.5 µL of PNPG-PEG (1 mg/mL) and 300 µL of TMB (10 mM) were added to different concentrations (0.1-15 mM) of H_2O_2 in acetate buffer (pH 4) at a final volume of 1.5 mL, and the reaction mixture was kept at 25°C for 30 min.

The effect of the temperature over the 25-55°C range, pH (2-10), and reaction time (5-30 min) was also investigated to evaluate their impact on the catalytic reaction. Thus, 37.5 µL of PNPG-PEG (1 mg/mL), 300 µL of TMB (10 mM) and 112.5 µL of H_2O_2 (100 mM) were

added to 1050 µL of acetate buffer at various temperatures, pH, and for various time intervals, respectively.

2.5. Kinetic analysis of PNPG-PEG nanoparticles

The Michaelis-Menten kinetics for PNPG-PEG nanoparticles were determined by selecting TMB and H_2O_2 as enzyme substrates. Thus, experiments were carried out by varying the concentration of one substrate (TMB or H_2O_2), while keeping constant the concentration of the other reagent. For TMB, the concentration was varied from 0.1 to 3 mM at constant H_2O_2 concentration (7.5 mM) at pH 4 and 35°C. For H_2O_2, the concentration was varied from 0.001 to 7.5 mM at constant TMB concentration (2 mM) at pH 4 and 35 °C.

The Lineweaver–Burk plots for PNPG-PEG nanoparticles were applied to calculate the important parameters in enzyme kinetics, such as K_m and V_m, using equation (1):

$$\frac{1}{V} = \frac{Km+[S]}{Vm\,[S]} = \frac{Km}{Vm}\,\frac{1}{[S]} + \frac{1}{Vm} \qquad (1)$$

V is the reaction rate, K_m is the Michaelis–Menten constant, V_m is the maximum reaction rate, and [S] is the substrate concentration [31].

2.6. Detection of Cr(VI) ions

To detect Cr(VI) ions, 37.5 µL of PNPG-PEG (1 mg/mL), 300 µL of TMB (10 mM) and 112.5 µL of H_2O_2 (100 mM) were added to different concentrations of Cr(VI) (0.01-12.5 µM) in acetate buffer (pH 4) at a final volume of 1.5 mL, and the reaction mixture was kept at 35°C. After 30 min, the change in absorption intensity at the wavelength of 655 nm was monitored and used for generating a calibration curve to determine the limit of detection, which was estimated based on the signal-to-noise ratio of the lowest concentration from 3 repeated measurements using the following formula (Eq. 2):

$$LOD = 3\sigma/S \qquad (2)$$

Where σ is the standard deviation of the lowest concentration and S is the slope of the calibration curve.

2.7. Selectivity and reproducibility

The selectivity of the developed technique was established against different interfering ions like Na(I), Pd(II), Ni(II), Zn(II), Cu(II), Mn(II), Mg(II), Cr(III), Fe(III) and Co(II) at a concentration of 5 or 10 µM in presence of Cr(VI). Thus 5 µM of Cr(VI) was mixed with different ions (5 or 10 µM), 37.5 µL of PNPG-PEG (1 mg/mL), 300 µL of TMB (10 mM) and 112.5 µL of H_2O_2 (100 mM), and the volume was adjusted to 1.5 mL using acetate buffer (pH 4). The resulting mixture was kept at 35°C for 30 min, and the absorbance intensity at 655 nm was recorded.

2.8. Detection of Cr(VI) ions in environmental water samples

The applicability of this method was examined by making a standard solution of Cr(VI) ions in environmental water samples from Parc Citadelle and Parc Roubaix Barbieux, Lille-France, using a standard addition method. To determine the Cr(VI) ion concentration in these environmental water samples, spiked concentrations of Cr(VI) (1, 5, and 10 µM) were added to 37.5 µL of PNPG-PEG (1 mg/mL), 300 µL of TMB (10 mM) and 112.5 µL of H_2O_2 (100 mM) and the volume was adjusted to 1.5 mL using acetate buffer (pH 4). The reaction mixture was kept at 35°C for 30 min and the absorbance intensity at 655 nm was recorded.

2.9. Reusability of PNPG-PEG nanoparticles

The reusability of the PNPG-PEG nanoparticles was determined up to four consecutive repeated cycles. To perform this study, 37.5 µL of PNPG-PEG (1 mg/mL), 300 µL of TMB (10 mM) and 112.5 µL of H_2O_2 (100 mM) were added to 10 µM of Cr(VI); the volume was adjusted to 1.5 mL using acetate buffer (pH 4). The reaction mixture was kept at 35°C for 30 min, and then centrifuged at 13,500 rpm for 15 min. The supernatant was separated and the

absorbance intensity at 655 nm was determined. The precipitate was rinsed with deionized water, dried and used again for the next catalytic cycle.

2.10. The investigation of the mechanism

To assess the mechanism towards the formation of an oxidized TMB product enhanced by the generation of hydroxyl radicals ($HO^{\bullet}$) from the reaction between PNPG-PEG, H_2O_2 and Cr(VI), terephthalic acid (TA) was chosen as a probe molecule. In the presence of $HO^{\bullet}$, TA generates a fluorescent product (HTA), which can be observed through fluorescence spectroscopy by displaying a fluorescent emission peak at 410 nm.

In a typical procedure TA (0.15 mM) in DMSO was added to (a) H_2O_2 (7.5 mM), (b) Cr (VI) (10 µM), (c) PNPG-PEG nanoparticles (25 µg/mL), (d) H_2O_2 (7.5 mM) + PNPG-PEG nanoparticles (25 µg/mL), (e) H_2O_2 (7.5 mM) + Cr(VI) (10 µM), (f) Cr(VI) (10 µM) + PNPG-PEG nanoparticles (25 µg/mL), (g) H_2O_2 (7.5 mM) + Cr(VI) (10 µM) + PNPG-PEG nanoparticles (25 µg/mL) in 1.5 mL acetate buffer (pH 4) and kept at 35°C for 30 min. The emission fluorescence spectra were then recorded in the range of 395-550 nm using an excitation wavelength (λ_{ex}) of 315 nm.

ROS scavenging experiment was also conducted using isopropanol to confirm the generation of OH radicals. Thus, to a mixture of PNPG-PEG (25 µg/mL), H_2O_2 (7.5 mM) and TMB (2 mM) was added 1 mM of isopropanol in acetate buffer (0.1 M, pH 4) and incubated for 30 min at 35 °C. The absorbance at 655 nm was then recorded by UV-vis spectrophotometry.

3. Results and discussion

3.1. Characterization of PNPG-PEG nanoparticles

Figure 1 depicts the FTIR spectra of PNPG and PNPG-PEG nanoparticles. The FTIR spectrum of PNPG nanoparticles comprises a broad band at ~3439 cm^{-1} due to the stretching of OH in carboxylic acid groups. The stretching bands at 1664 and 1592 cm^{-1} are due to

carbonyl group and quinoid rings, respectively. The stretching band at 1504 cm^{-1} is ascribed to the benzenoid rings. The peak at 1308 cm^{-1} is assigned to C–N stretching vibration and the bands at 1146 and 828 cm^{-1} are characteristic vibrational modes of quinoid ring (in-plane C–H and C–H out-of-plane bending vibrations, respectively). Similarly, the FTIR spectrum of PNPG-PEG nanoparticles exhibits a broad band at 3443 cm^{-1} ascribed to OH stretching vibration. The stretching vibration at 1651 cm^{-1} is due to carbonyl–amide bond, while the bands at 1559 and 1484 cm^{-1} are typical of quinoid and benzenoid stretchings, respectively. The C=N stretching vibration in the quinoid units is observed at 1401 cm^{-1}. The band at 1306 cm^{-1} is ascribed to the C–N stretching vibrations and the peaks at 1103 and 800 cm^{-1} are characteristic vibrational modes of quinoid ring (in-plane C–H and C–H out-of-plane bending vibrations, respectively) [30].

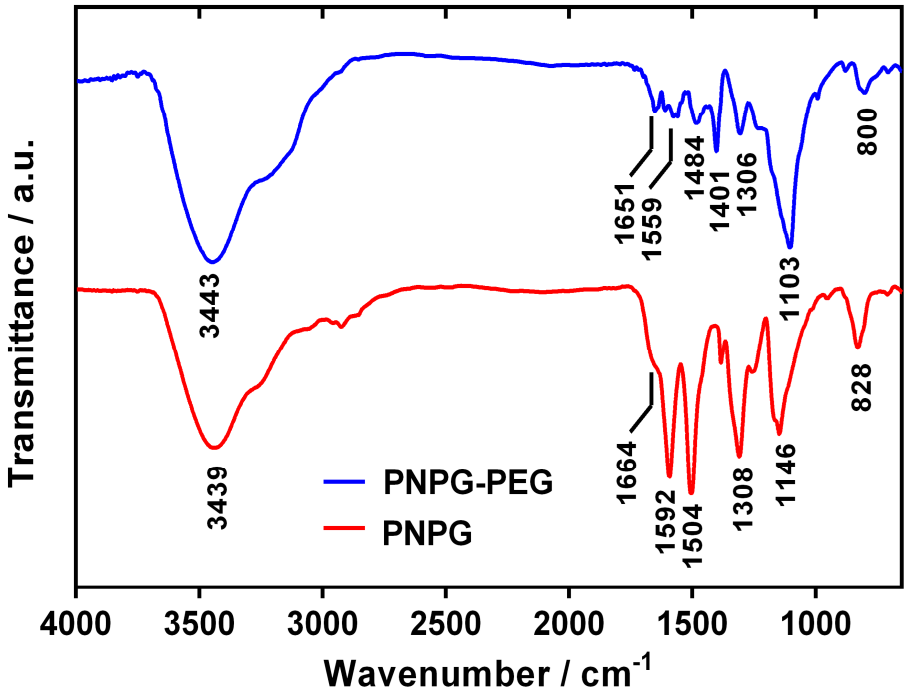

Figure 1. FTIR spectra of PNPG and PNPG-PEG nanoparticles.

The thermal stability of PNPG and PNPG-PEG nanoparticles was assessed by thermogravimetric analysis (TGA) measurements in the 30–980°C temperature range under N_2 atmosphere (**Fig. S1A**). The TGA curve of PNPG nanoparticles depicts three separated

weight losses at temperatures of: (I) 100°C, (II) 285°C, and (III) 510°C, which are attributed to (I) water evaporation, (II) carboxylic acid (COOH) groups decomposition, and (III) PNPG backbone degradation (**Fig. S1B**). Interestingly, the thermogram of PNPG-PEG nanoparticles showed much smaller weight loss at 285°C (II) (**Fig. S1C**). This decreased of weight loss demonstrates that a large fraction of carboxylic acid groups is substituted by carboxamide (CONRR') groups. The weight loss recorded at (III) 370°C and (IV) 510°C are most likely due to the decomposition of the PEG and PNPG backbones, respectively [30, 32].

Zeta potential measurements were recorded to examine the surface charge of PNPG-PEG nanoparticles. A mean potential value of +17.5 mV was recorded for PNPG-PEG nanoparticles (**Fig. S2A**). The mean hydrodynamic size of PNPG-PEG nanoparticles was 290 nm, as revealed by dynamic light scattering (DLS) measurements (**Fig. S2B**).

The morphology of PNPG-PEG nanoparticles was assessed by scanning electron microscopy (SEM), revealing that the PNPG-PEG nanoparticles have a nearly spherical shape with an average diameter ranging between 85 and 107 nm (**Fig. 2**).

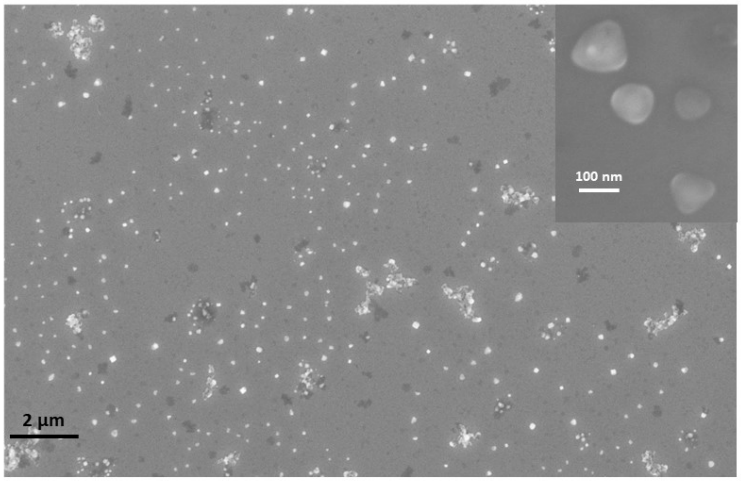

Figure 2. SEM images at low (a) and high (b) magnifications of PNPG-PEG nanoparticles.

The elemental composition along with the oxidation state of different surface elements of PNPG-PEG were investigated by X-ray photoelectron spectroscopy (XPS). In the XPS survey spectrum of PNPG-PEG (**Fig. S3A**), bands at 284.2 eV (C_{1s}), 531.8 eV (O_{1s}), and 399 eV

(N_{1s}) are clearly visible, in full agreement with the composition of PNPG. The C_{1s} spectrum **(Fig. S3B)** reveals bands at binding energies of 284.0 eV (C_{sp2}), 284.7 eV (C_{sp3}), 285.6 eV (C-N/C-O), and a peak at 287.4 eV ascribed to C=O/C=N. The high resolution of the N_{1s} spectrum shows bands at binding energies of 399.1 and 401.7 eV attributed to C-N-C and C=N-C, respectively **(Fig. S3C)**. The O_{1s} high resolution spectrum **(Fig. S3D)** can be deconvoluted with two components at 531.9 eV (C-O) and 534.1 eV (C=O).

3.2. Determination of peroxidase-like activity of PNPG-PEG nanoparticles

The peroxidase-like catalytic activity of PNPG-PEG nanoparticles (25 µg/mL) was assessed for the catalytic oxidation reaction of the TMB (1 mM) substrate in absence and presence of H_2O_2 (20 mM). As can be clearly seen from **Fig. 3**, in absence of H_2O_2, PNPG-PEG nanoparticles were not effective for TMB oxidation in acetate buffer (pH 4).

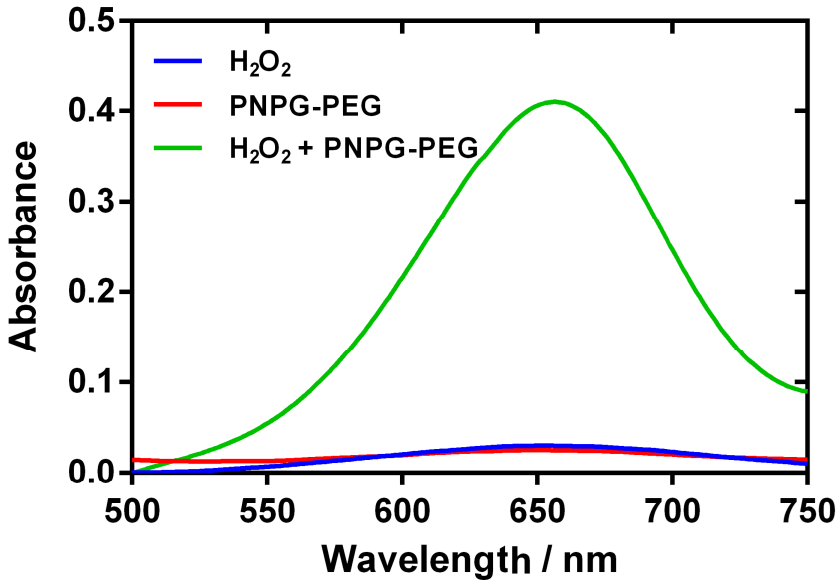

Figure 3. UV–vis absorbance spectra of TMB (1 mM) in presence of H_2O_2 (20 mM) (blue), PNPG-PEG (25 µg/mL) (red), H_2O_2 (20 mM) + PNPG-PEG (25 µg/mL) (green).

However, addition of PNPG-PEG to a TMB/H_2O_2 mixture produces a blue color solution due to the oxidation of TMB to TMBDI; the latter displays an absorption band with a maximum at

~655 nm (**Fig. 3**) [33]. The result indicates that PNPG-PEG and H_2O_2 are responsible to carry out this catalytic reaction, similar to the Fenton reaction.

The catalytic activity of PNPG-PEG nanoparticles towards TMB catalytic oxidation is influenced by the amount of catalyst, pH, and temperature [34]. **Figure 4A** displays the effect of PNPG-PEG concentration on TMB oxidation in the presence of H_2O_2. The results clearly show that the optimal activity (highest absorbance maximum at ~655 nm) was achieved at a PNPG-PEG concentration of 25 µg/mL.

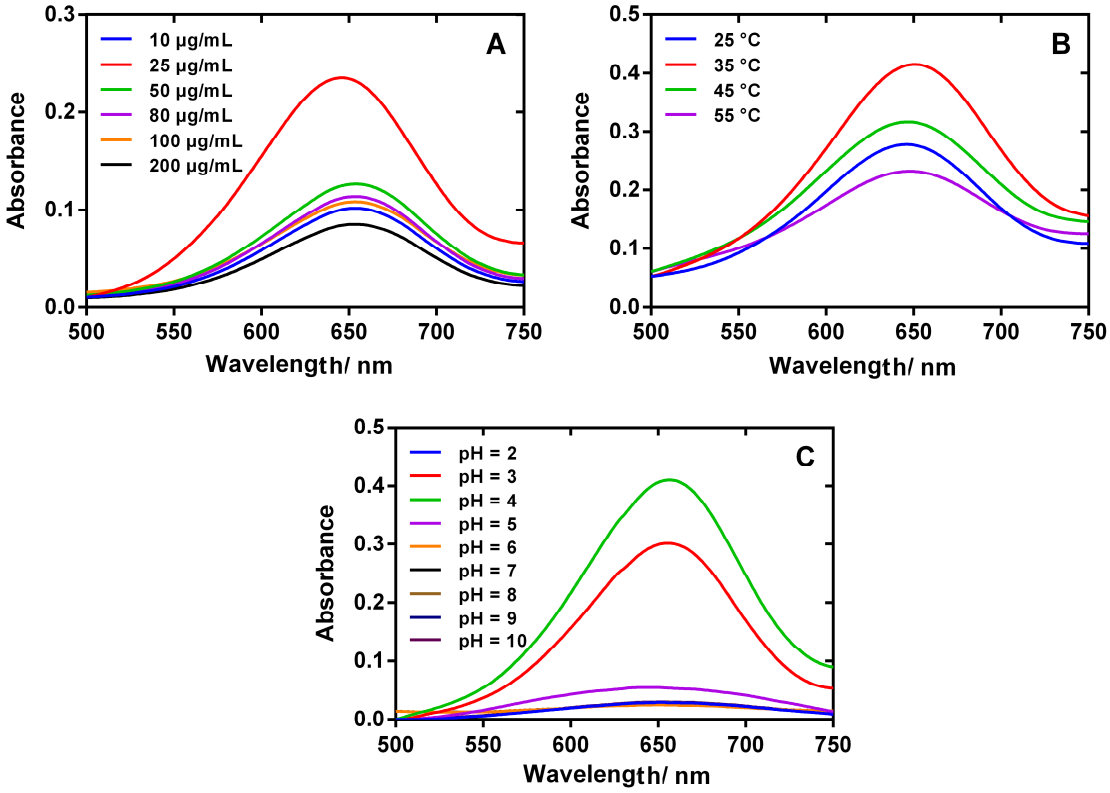

Figure 4. (A) UV–vis absorbance spectra of TMB at different PNPG-PEG concentrations, TMB (1 mM), H_2O_2 (20 mM), T=25 °C, pH=4; (B) UV–vis absorption spectra of TMB as a function of temperature, PNPG-PEG (25 µg/mL), TMB (2 mM), H_2O_2 (7.5 mM), pH=4; (C) UV–vis absorption spectra of TMB at different pH values, PNPG-PEG (25 µg/mL), TMB (2 mM), H_2O_2 (7.5 mM), T=35°C.

At higher catalyst concentrations, a decrease in absorption was observed due most likely to nanoparticles' aggregation, leading to a decrease in the number of available active sites. The influence of temperature on the catalytic activity of the PNPG-PEG catalyst is displayed in **Fig. 4B**, where the maximum absorbance was attained at 35°C. The decomposition of H_2O_2 at temperatures ranging from 35ºC to 50ºC leads to a decrease in enzyme-like activity. Similarly, as observed in **Fig. 4C**, the maximum catalytic activity of the catalyst was achieved at pH 4. Thus, our optimum conditions were found at pH 4, 35°C and 25 µg/mL of PNPG-PEG nanoparticles.

3.3. Kinetic study of PNPG-PEG nanoparticles as the peroxidase-like enzyme - Determination of Michaelis constant

To comprehend the enzyme function, a kinetic description of its activity is necessary to establish. The Michaelis-Menten kinetic model is the one of the best-known methods to describe enzyme kinetics. For many enzymes, the rate of catalysis varies with the substrate concentration. In this work, the peroxidase-like catalytic activity of PNPG-PEG nanoparticles was assessed by varying the concentration of TMB or H_2O_2, while maintaining the concentration of the other reagent constant. The Michaelis-Menten curves for TMB and H_2O_2 are displayed in **Fig. 5A** and **Fig. 5B**, respectively. The values of Michaelis constant (K_m) and maximal velocity (V_m) for PNPG-PEG nanoparticles were determined from the Lineweaver Burk double reciprocal plots (**Fig. 5A, B insets**). The values of K_m and V_m for PNPG-PEG nanoparticles and other catalysts are displayed in **Table 1**. The K_m value of 0.2828 for TMB, and 0.0799 for H_2O_2 recorded by PNPG-PEG nanoparticles evidences that TMB oxidation occurs at lower concentrations of H_2O_2 as compared to other enzymes.

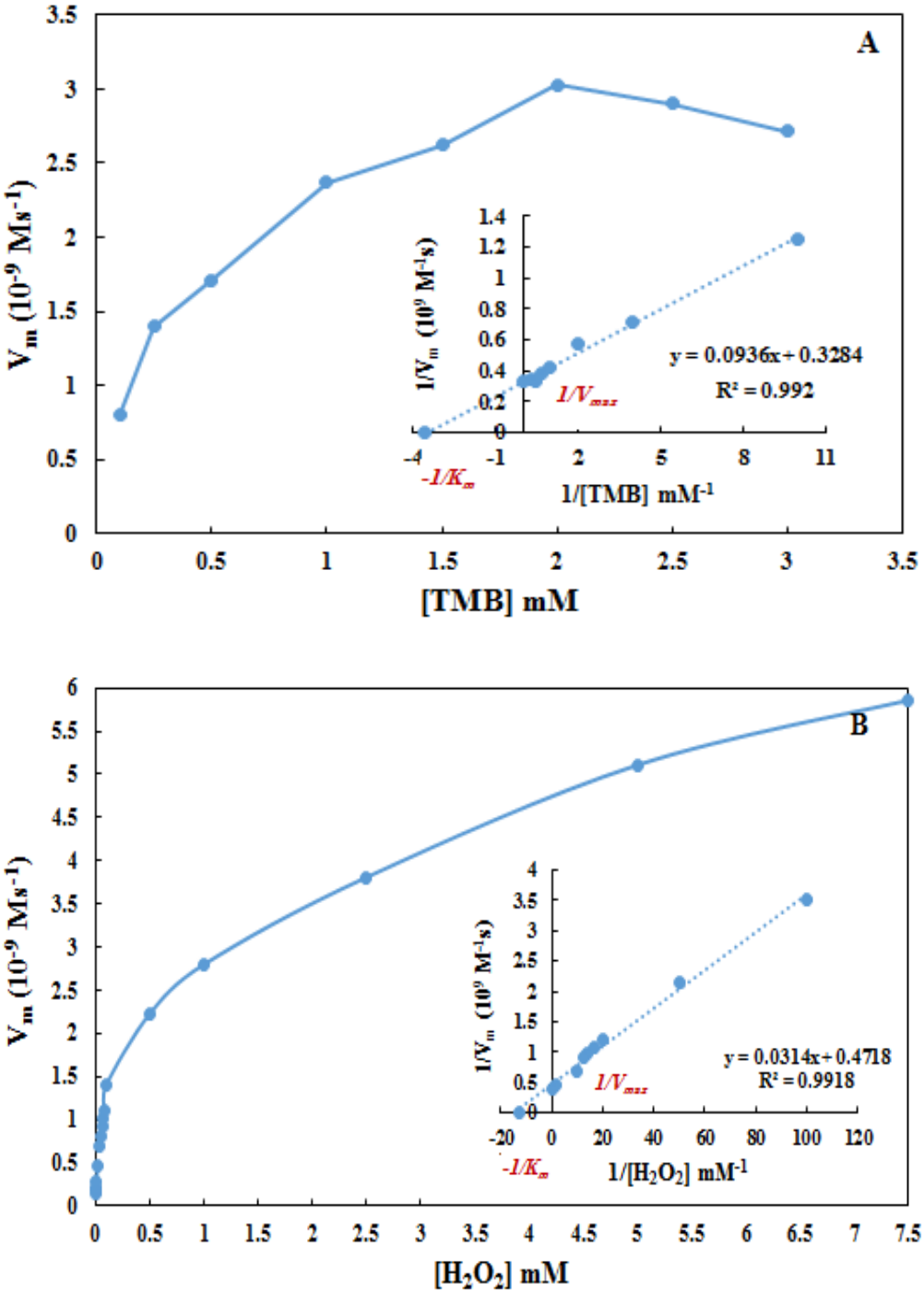

Figure 5. Steady-state kinetics of PNPG-PEG nanoparticles: (A) varying the concentration of TMB (0.1–3 mM), [H_2O_2] =7.5 mM; (B) varying the concentration of H_2O_2 (0.001–7.5 mM), [TMB]=2 mM. The Lineweaver Burk double reciprocal plots are shown in the inset.

Table 1. Steady-state kinetic parameters: Michaelis Menten constant (K_m) and maximum velocity (V_m) for PNPG-PEG and other polymer/metal nanoparticles.

Catalysts	Substrates	K_m (mM)	V_m (10^{-9} Ms^{-1})	Ref.
PANi–MnO_2–Pd	H_2O_2	2.55	172.8	[35]
PANi–MnO_2–Pd	TMB	0.13	300.24	[35]
MoS_2/PPy	H_2O_2	12.8	151	[36]
MoS_2/PPy	TMB	0.41	474	[36]
CeO_2/Co_3O_4/PEDOT	H_2O_2	0.12	-	[29]
CeO_2/Co_3O_4/PEDOT	TMB	1.26	-	[29]
PPy	H_2O_2	0.027	11.7	[28]
PPy	TMB	0.2157	12.9	[28]
PNPG-PEG	H_2O_2	0.0799	2.467	This work
PNPG-PEG	TMB	0.2828	3.0276	This work

3.4. Colorimetric sensing of Cr(VI) ions using PNPG-PEG nanozyme

Finally, the possibility of Cr(VI) sensing using PNPG-PEG nanozyme was investigated. Addition of PNPG-PEG to a TMB/H_2O_2 mixture produces a blue color solution due to the generation of hydroxyl radicals that are responsible for the oxidation of TMB to TMBDI. This solution displays an absorption band with a maximum at ~655 nm. **Fig. 6A** clearly shows that the catalytic oxidation of TMB is enhanced in presence of Cr(VI) ions at low pH, which is most likely due to the decomposition of H_2O_2 into H_2O and O_2 by Cr(VI) [25, 26]. Subsequently, PNPG-PEG nanozyme combines with O_2 and H_2O to produce hydroxyl radicals ($HO^{\bullet}$). These reactive hydroxyl radicals can oxidize TMB to blue colored TMBDI [23].

The relationship between the Cr(VI) concentration *vs.* absorbance intensity changes of TMBDI is displayed in **Fig. 6B**. The sensor displays two linear ranges from 0.01 to 0.1 µM and from 0.05 to 12.5 µM with respective detection limits of 0.012 µM and 0.52 µM using **Eq. 2**. In **Table 2**, the detection limit and linear range of the developed colorimetric sensor is compared with other detection techniques such as electrochemistry [8, 10, 37], fluorescence [13, 14], and colorimetry [21, 23, 25, 38]. It is clear that the developed PNPG-PEG nanozyme outperforms the different sensors reported for Cr(VI) detection using different means.

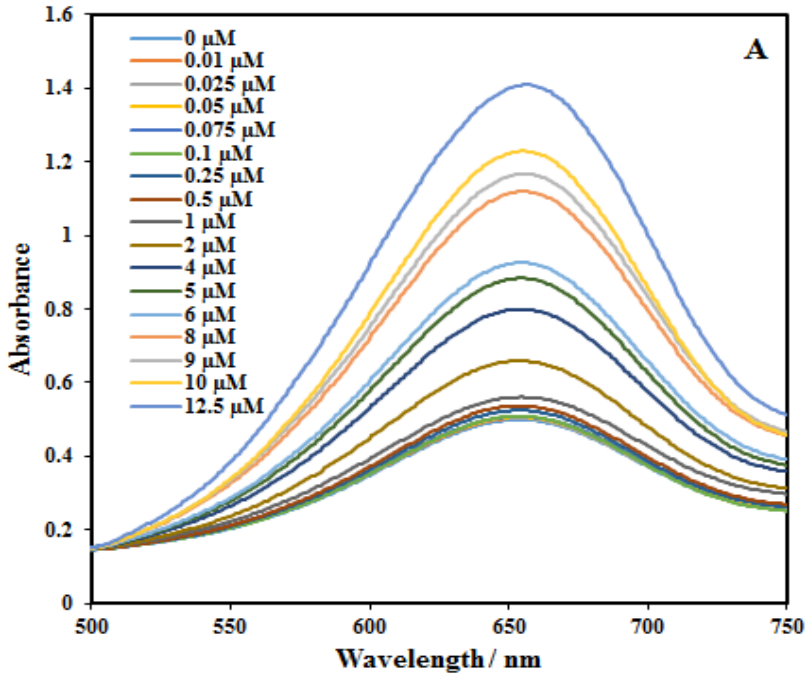

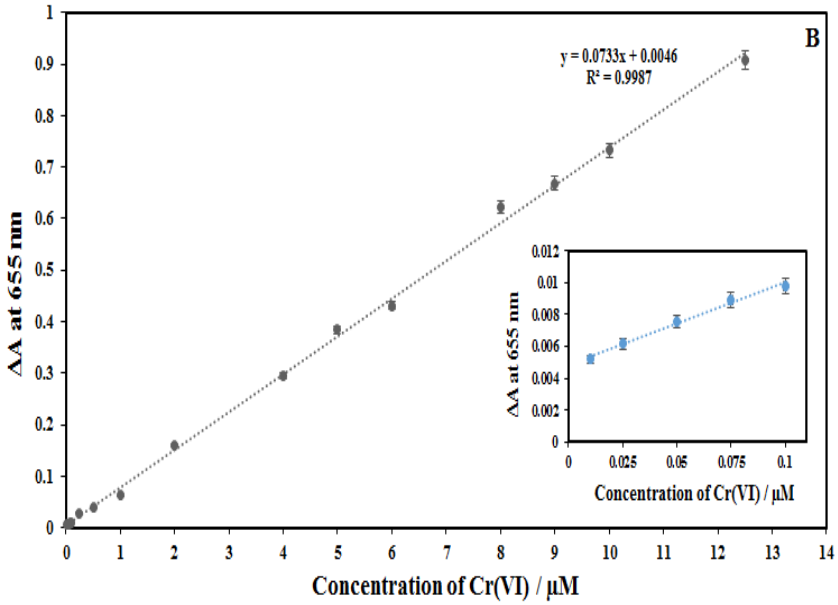

Figure 6. (A) UV–vis absorbance spectra of oxTMB in absence and presence of Cr(VI) ions, reaction conditions: TMB (2 mM), PNPG-PEG (25 µg/mL), of H_2O_2 (7.5 mM), T=35°C, pH=4; (B) Plots of the absorbance intensity changes at 655 nm *versus* Cr(VI) concentration. Plots of the absorbance intensity changes at 655 nm *versus* lower concentrations of Cr(VI) shown in the inset

The selectivity of the proposed method was evaluated in presence of different interfering ions like Na(I), Pd(II), Ni(II), Zn(II), Co(II), Cu(II), Mn(II), Ca(II), Mg(II), Cr(III) and Fe(III) ions at 5 or 10 µM in presence of 5 µM Cr(VI) ion. As shown in **Fig. 7**, the absorbance of oxTMB at 655 nm was not significantly affected by the presence of other metal ions except Fe(III), suggesting that the PNPG-PEG nanozyme displays good selectivity for Cr(VI) ions.

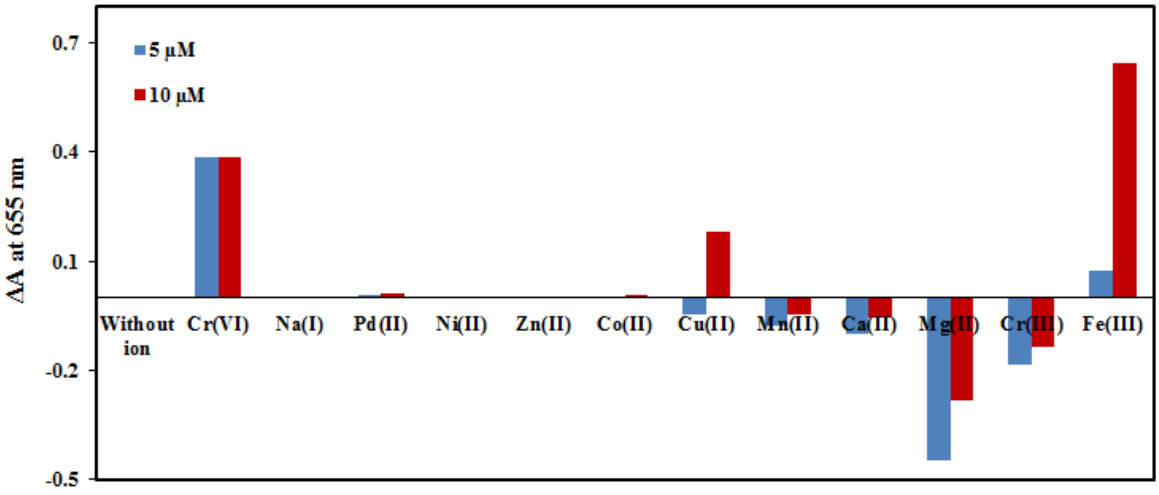

Figure 7. Plots of oxTMB absorbance changes at 655 nm in presence of different interfering ions at concentrations of 5 and 10 µM of Na(I), Pd(II), Ni(II), Zn(II), Co(II), Cu(II), Mn(II), Ca(II), Mg(II), Cr(III) and Fe(III) ions and 5 µM of Cr(VI); reaction conditions: TMB (2 mM), PNPG-PEG (25 µg/mL), H_2O_2 (7.5 mM), T=35°C, pH=4.

Table 2. Comparison of analytical efficiency of the developed sensor with different methods.

Method	Linear range (µM)	Detection limit (µM)	Ref.
Electrochemistry	0.8–230	0.72	[10]
Electrochemistry	0.35–40	0.10	[37]
Fluorescence	1–400	0.13	[13]
Colorimetric	0.1–20	0.088	[38]
Colorimetric	0.577-57.7	0.44	[24]
Colorimetric	0.5–50	0.280	[21]
Colorimetric	0–0.2	0.067	[23]
Colorimetric	0.01–0.1	0.012	This work
Colorimetric	0.05–12.5	0.52	This work

3.5. Sensing Cr(VI) ions in spiked environmental samples

To demonstrate the practical applicability of this method, the colorimetric determination of Cr(VI) was examined in environmental water samples. The percentage of recovery and relative standard deviation (RSD) are presented in **Table 3** (n = 3). These results reveal the potential of the developed technique for Cr(VI) quantification in real samples.

Table 3. The recovery of Cr(VI) ions in environmental water samples (n = 3).

Samples	Cr(VI) added (µM)	Cr(VI) found (µM)	RSD (%)	Recovery (%)
Parc Citadelle Lille	1	1.09	0.788	109.0
	5	5.2	0.534	104.0
	10	11.1	0.848	111.0
Parc Roubaix Barbieux	1	0.99	0.395	99.0
	5	5.4	0.496	108.0
	10	9.96	0.389	99.6

3.6. Reusability of PNPG-PEG nanoparticles

To perform this study, 37.5 µL of PNPG-PEG (1 mg/mL), 300 µL of TMB (10 mM) and 112.5 µL of H_2O_2 (100 mM) were added to 10 µM of Cr(VI) in acetate buffer (pH 4) to a final volume of 1.5 mL, and the mixture was kept at 35°C for 30 min. Then the mixture was centrifuged at 13,500 rpm for 15 min. The supernatant was removed and the absorbance intensity at 655 nm was recorded. The precipitate was washed with deionized water, dried and used again for the next cycle. As shown in **Fig. 8**, the catalytic efficiency of PNPG-PEG nanoparticles decreased slightly with increasing the number of cycles. This result indicates that the PNPG-PEG nanoparticles exhibit a good reusability during the catalytic reaction.

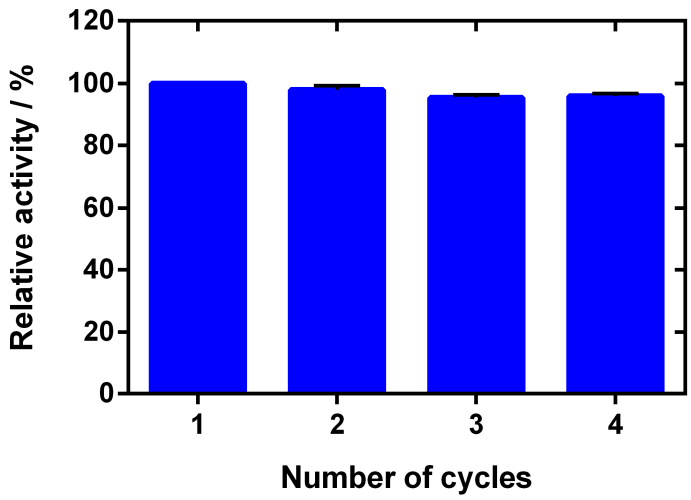

Figure 8. Catalytic activity of PNPG-PEG nanoparticles for four successive repeated cycles.

3.7. The investigation of the catalytic reaction mechanism

To gain a better understanding on the formation of hydroxyl radicals (•OH) reactive intermediates, fluorescence spectroscopy was recorded using terephthalic acid (TA), as a fluorescence probe. TA reacts readily with hydroxyl radicals to produce a highly fluorescent 2-hydroxy terephthalic acid (HTA, λ_{em} ~ 435 nm). In this experiment, the production of hydroxyl radicals by PNPG-PEG nanoparticles in presence of H_2O_2 is directly evidenced by the increase of the fluorescence intensity (**Fig. 9**). This contrasts with the low fluorescence intensity recorded in absence of H_2O_2 or H_2O_2 alone. Also, the significant enhancement of the fluorescence intensity recorded in presence of 10 µM Cr(VI) attests that Cr(VI) can increase the decomposition of H_2O_2 to H_2O and O_2, which can accept electrons from the nanoparticles surface to generate hydroxyl radicals (•OH):

$$H_2O_2 \xrightarrow{Cr(VI)} H_2O + O_2$$

$$H_2O + O_2 \xrightarrow{PNPG\text{-}PEG\ NPs} {}^{\bullet}OH$$

$$TA\ (non\text{-}\ fluorescent) \xrightarrow{{}^{\bullet}OH} HTA\ (fluorescent,\ 435\ nm)$$

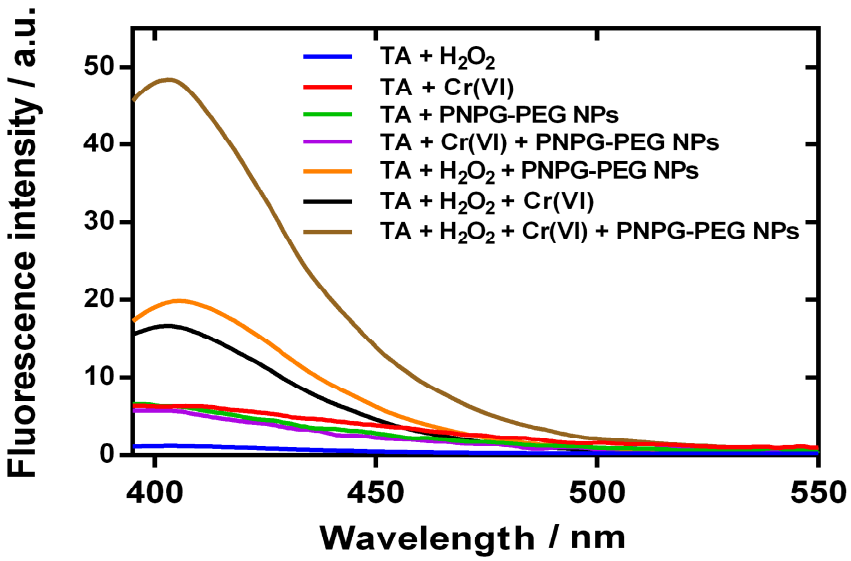

Figure 9. Fluorescence emission spectra recorded at λ_{ex}= 315 nm to identify catalytic reaction mechanism; reaction conditions: TA (0.15 mM in DMSO), H_2O_2 (7.5 mM), Cr(VI) (10 µM), PNPG-PEG nanoparticles (25 µg/mL), T=35°C, pH 4 in 1400 µL of water and 100 µL of DMSO.

The oxidation of TMB was also examined in the presence of ROS scavengers, such as isopropanol, that is readily known to quench •OH radicals. To perform this study, to a mixture of PNPG-PEG (25 µg/mL), H_2O_2 (7.5 mM) and TMB (2 mM), 1 mM of isopropanol was added in acetate buffer (0.1 M, pH 4) and kept for 30 min at 35°C. It is clearly observed from **Fig. 10** that isopropanol lowers the rate of the enzymomimetic action of PNPG-PEG nanoparticles both in absence and presence of Cr(VI). This indicates that the •OH radicals are the main reactive species for TMB oxidation.

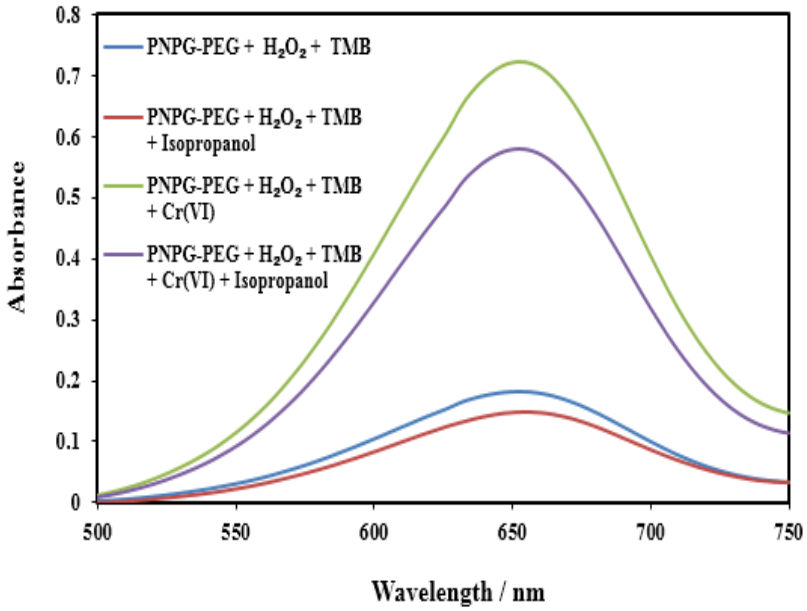

Figure 10. Effect of isopropanol on the catalytic activity of PNPG-PEG nanoparticles. Reaction conditions: TMB (2 mM), PNPG-PEG (25 µg/mL), H_2O_2 (7.5 mM), isopropanol (1 mM), T=35°C, pH=4.

Although the use of polymer nanoparticles as a peroxidase mimic represents an appealing method for the colorimetric detection of different analytes and adds to the list of the many developed inorganic particles in the field of nanozymes, the enhanced peroxidase activity was recorded only in acidic media like for most nanozymes. This is certainly a limiting factor for the practical applications of the nanozyme in sensing or generation of hydroxyl radicals in biological media or for *in vivo* investigations.

4. Conclusion

In conclusion, we synthesized water dispersible polyethylene glycol-functionalized poly(N-phenylglycine) (PNPG-PEG) nanoparticles and investigated their enzyme-like catalytic activity. In comparison to other nanocomposites and nanoparticles, PNPG-PEG nanoparticles displayed highly efficient peroxidase-like activity. Additionally, the enhanced peroxidase-like activity of PNPG-PEG was evaluated for the detection of Cr(VI). The sensor achieved a detection limit of 0.012 µM (0.01-0.1 µM linear range) and 0.52 µM (0.05-12.5

μM linear range). The method was highly selective and successfully applied for Cr(VI) sensing in real samples. The usage of polymer nanoparticles holds great promise for enzyme-like sensing of various chemical and biological species, owing to their diverse functionalities, good electrical conductivity and redox properties.

Acknowledgement

SG, AS, AB, SS and RB acknowledge financial support from the Centre National de la Recherche Scientifique (CNRS), the University of Lille, the Hauts-de-France region and the CPER "Photonics for Society".

References

[1] P.B. Tchounwou, C.G. Yedjou, A.K. Patlolla, D.J. Sutton, Heavy Metals Toxicity and the Environment, Mol. Clin. Environ. Toxicol., 101 (2012) 133-164.

[2] H. Oliveira, Chromium as an Environmental Pollutant: Insights on Induced Plant Toxicity, Jpn. J. Bot., 2012 (2012) 1-8.

[3] F.N. Acar, E. Malkoc, The Removal of Chromium(VI) From Aqueous Solutions by Fagus orientalis L., Bioresource Technol., 94 (2004) 13-15.

[4] T.N. De Castro Dantas, A.A. Dantas Neto, M.C.P. De A. Moura, Removal of Chromium From Aqueous Solutions by Diatomite Treated with Microemulsion, Water Res., 35 (2001) 2219-2224.

[5] S.K. Ouki, R.D. Neufeld, Use of Activated Carbon for the Recovery of Chromium From Industrial Wastewaters, J. Chem. Tech. Biotechnol., 70 (1997) 3-8.

[6] M.M. Loock, J.P. Beukes, P.G. Van Zyl, A Survey of Cr (VI) Contamination of Surface Water in the Proximity of Ferrochromium Smelters in South Africa, Water S A, 40 (2014) 709–716.

[7] Guidance for Drinking Water Quality, WHO, 1 (1993) 45-46.

[8] D.P. Jaihindh, B. Thirumalraj, S.M. Chen, P. Balasubramanian, Y.P. Fu, Facile Synthesis of Hierarchically Nanostructured Bismuth Vanadate: An Efficient Photocatalyst for Degradation and Detection of Hexavalent Chromium, J. Hazard. Mater., 367 (2019) 647-657.

[9] J. Tu, Y. Gan, T. Liang, H. Wan, P. Wang, A Miniaturized Electrochemical System For High Sensitive Determination of Chromium(VI) by Screen-Printed Carbon Electrode with Gold Nanoparticles Modification, Sens. Actuators B, 272 (2018) 582-588.

[10] C.B. Breslin, D. Branagan, L.M. Garry, Electrochemical Detection of Cr(VI) with Carbon Nanotubes Decorated with Gold Nanoparticles, J. Appl. Electrochem., 49 (2019) 195-205.

[11] C.X. Wang, Y.P. Xia, Z.Q. Yao, J. Xu, Z. Chang, X.H. Bu, Two Luminescent Coordination Polymers as Highly Selective and Sensitive Chemosensors for CrVI-Anions in Aqueous Medium, Dalton Trans., 48 (2019) 387-394.

[12] Y. Jin, Y. Sun, C. Li, C. Yang, A Highly Selective Chemiluminescent Probe for the Detection of Chromium(VI), Spectrochim. Acta A, 192 (2018) 82-87.

[13] F.P. Mutuyimana, J. Liu, S. Nsanzamahoro, M. Na, H. Chen, X. Chen, Yellow-emissive Carbon dots as a Fluorescent Probe for Chromium(VI), Microchim. Acta, 186 (2019) 163.

[14] Y. Ma, Y. Chen, J. Liu, Y. Han, S. Ma, X. Chen, Ratiometric Fluorescent Detection of Chromium(VI) in Real Samples Based on Dual Emissive Carbon Dots, Talanta 185 (2018) 249-257.

[15] A.S. Passos, G.F. Tonon, F.V. Nakadi, A.S. Mangrich, J.B. Andrade, B. Welzde, M.G.R. Vale, Determination of Cr, Cu and Pb in Industrial Waste of Oil Shale Using High-Resolution Continuum Source Graphite Furnace Atomic Absorption Spectrometry and Direct Solid Sample Analysis, Microchem. J., 10 (2018) 3645-3653.

[16] S. Parvizi, M. Behbahani, F. Zeraatpisheh, A. Esrafili, Preconcentration and Ultra-trace Determination of Hexavalent Chromium Ions Using Tailor-made Polymer Nanoparticles

Coupled with Graphite Furnace Atomic Absorption Spectrometry: Ultrasonic Assisted-Dispersive Solid-Phase Extraction, New J. Chem., 42 (2018) 10357-10365.
[17] J. Renpenning, S. Kummel, K.L. Hitzfeld, A. Schimmelmann, M. Gehre, Compound-Specific Hydrogen Isotope Analysis of Heteroatom-Bearing Compounds via Gas Chromatography-Chromium-Based High-Temperature Conversion (Cr/HTC)-Isotope Ratio Mass Spectrometry, Anal. Chem., 87 (2015) 9443-9450.
[18] D.P. Bishop, D.J. Hare, D. Clases, P.A. Doble, Applications of Liquid Chromatography-Inductively Coupled Plasma-Mass Spectrometry in the Biosciences: A Tutorial Review and Recent Developments, Trac-Trend. Anal. Chem., 104 (2018) 11-21.
[19] J. Sun, Z. Yang, H. Leea, L. Wang, Simultaneous Speciation and Determination of Arsenic, Chromium and Cadmium in Water Samples by High Performance Liquid Chromatography with Inductively Coupled Plasma Mass Spectrometry, Anal. Methods, 7 (2015) 2653-2658.
[20] C. Dong, G. Wu, Z. Wang, W. Ren, Y. Zhang, Z. Shen, T. Lib, A. Wu, Selective Colorimetric Detection of Cr(III) and Cr(VI) Using Gallic Acid Capped Gold Nanoparticles, Dalton Trans., 45 (2016) 8347-8354.
[21] J.F. Guo, D.Q. Huo, M. Yang, C.J. Hou, J.J. Li, H.B. Fa, H.B. Luo, P. Yang, Colorimetric Detection of Cr(VI) Based on the Leaching of Gold Nanoparticles Using a Paper-based Sensor, Talanta, 161 (2016) 819-825.
[22] N.N. Nghia, B.T. Huy, Y.I. Lee, Colorimetric Detection of Chromium(VI) Using Graphene Oxide Nanoparticles Acting as a Peroxidase Mimetic Catalyst and 8-Hydroxyquinoline as an Inhibitor, Microchim. Acta, 186 (2019) 36.
[23] P. Borthakur, P.K. Boruah, M.R. Das, S. Szunerits, R. Boukherroub, Cu(0) Nanoparticle-decorated Functionalized Reduced Graphene Oxide Sheets as Artificial Peroxidase Enzymes: Application for Colorimetric Detection of Cr(VI) Ions, New J. Chem., 43 (2019) 1404-1414.

[24] P. Borthakur, P.K. Boruah, M.R. Das, S.B. Artemkina, P.A. Poltarakcd, V.E. Fedorov, Metal-free MoS_2 2D Sheets as a Peroxidase Enzyme and Visible-light-induced Photocatalyst Towards Detection and Reduction of Cr(VI) Ions, New J. Chem., 42 (2018) 16919-16929.

[25] A. Swaidan, P. Borthakur, P.K. Boruah, M.R. Das, A. Barras, S. Hamieh, J. Toufaily, T. Hamieh, S. Szunerits, R. Boukherroub, A Facile Preparation of CuS-BSA Nanocomposite as Enzyme Mimics: Application for Selective and Sensitive Sensing of Cr(VI) Ions, Sens. Actuators B, 294 (2019) 253-262.

[26] P. Borthakur, M.R. Das, S. Szunerits, R. Boukherroub, CuS Decorated Functionalized Reduced Graphene Oxide: A Dual Responsive Nanozyme for Selective Detection and Photoreduction of Cr(VI) in an Aqueous Medium, ACS Sustainable Chem. Eng., 7 (2019) 16131-16143.

[27] M. Liu, B. Li, X. Cui, Anionic Polythiophene Derivative as Peroxidase Mimetics and Their Application for Detection of Hydrogen Peroxide and Glucose, Talanta 115 (2013) 837-841.

[28] Y. Tao, E. Ju, J. Ren, X. Qu, Polypyrrole Nanoparticles as Promising Enzyme Mimics for Sensitive Hydrogen Peroxide Detection, Chem. Commun., 50 (2014) 3030-3032.

[29] Z. Yang, C. Wang, X. Lu, Conducting Polymer-based Peroxidase Mimics: Synthesis, Synergistic Enhanced Properties and Applications, Sci. China Mater., 61 (2018) 653-670.

[30] B.P. Jiang, L. Zhang, X.L. Guo, X.C. Shen, Y. Wang, Y. Zhu, H. Liang, Poly(N-phenylglycine)-Based Nanoparticles as Highly Effective and Targeted Near-Infrared Photothermal Therapy/Photodynamic Therapeutic Agents for Malignant Melanoma, Small, 13 (2017) 1602496.

[31] P.C. Engel, W. Ferdinand, The Significance of Abrupt Transitions in Lineweaver-Burk Plots with Particular Reference to Glutamate Dehydrogenase. Negative and Positive co-Operativity in Catalytic Rate Constants, Biochem. J., 131 (1973) 97-105.

[32] J.H. Doh, J.H. Kim, H.J. Kim, R.F. Ali, K. Shin, Y.J. Hong, Enhanced Adsorption of Aqueous Copper (II) Ions Using Dedoped Poly-N-Phenylglycine Nanofibers, Chem. Eng. J., 227 (2015) 352-359.

[33] G. Darabdhara, B. Sharma, M.R. Das, R. Boukherroub, S. Szunerits, Cu-Ag Bimetallic Nanoparticles on Reduced Graphene Oxide Nanosheets as Peroxidase Mimic for Glucose and Ascorbic Acid Detection, Sens. Actuators B, 238 (2017) 842-851.

[34] P. Borthakur, G. Darabdhara, M.R. Das, R. Boukherroub, S. Szunerits, Solvothermal Synthesis of CoS/Reduced Porous Graphene Oxide Nanocomposite for Selective Colorimetric Detection of Hg(II) Ion in Aqueous Medium, Sens. Actuators B, 244 (2017) 684-692.

[35] M. Zhong, M. Chi, F. Ma, Y. Zhu, C. Wang, X. Lu, Dual Responsive Enzyme Mimicking of Ternary Polyaniline-MnO_2-Pd Nanowires and Its Application in Colorimetric Biosensing, ACS Sustain. Chem. Eng., 6 (2018) 16482−16492.

[36] J. Lei, X. Lu, G. Nie, Z. Jiang, C. Wang, One-Pot Synthesis of Algae-Like MoS_2/PPy Nanocomposite: A Synergistic Catalyst with Superior Peroxidase-Like Catalytic Activity for H_2O_2 Detection, Part. Part. Syst. Charact., 32 (2015) 886-892.

[37] Z. Stojanovic, Z. Koudelkova, E. Sedlackova, D. Hynek, L. Richtera, V. Adam, Determination of Chromium(VI) by Anodic Stripping Voltammetry Using a Silver-plated Glassy Carbon Electrode, Anal. Methods, 10 (2018) 2917-2923.

[38] F.M. Li, J.M. Liu, X.X. Wang, L.P. Lin, W.L. Cai, X. Lin, Y.N. Zeng, Z.M. Li, S.Q. Lin, Non-Aggregation Based Label Free Colorimetric Sensor for the Detection of Cr (VI) Based on Selective Etching of Gold Nanorods, Sens. Actuators B, 155 (2011) 817-822.

Graphical Abstract